PHYSICAL REVIEW B **79**, 165208 (2009)

Ferromagnetism and spin-polarized charge carriers in In_2O_3 thin films

Raghava P. Panguluri,[1] P. Kharel,[1] C. Sudakar,[1] R. Naik,[1] R. Suryanarayanan,[1,*] V. M. Naik,[2] A. G. Petukhov,[3] B. Nadgorny,[1] and G. Lawes[1]

[1]*Department of Physics and Astronomy, Wayne State University, Detroit, Michigan 48201, USA*

[2]*Department of Natural Sciences, University of Michigan-Dearborn, Dearborn, Michigan 48128, USA*

[3]*Department of Physics, South Dakota School of Mines, Rapid City, South Dakota 57701, USA*

(Received 2 March 2009; published 27 April 2009)

We present evidence for spin-polarized charge carriers in In_2O_3 films. Both In_2O_3 and Cr doped In_2O_3 films exhibit room-temperature ferromagnetism after vacuum annealing, with a saturation moment reaching approximately 0.5 emu/cm^3 for the Cr doped samples. We used point contact Andreev reflection measurements to directly determine the spin polarization, which was found to be approximately $50\% \pm 5\%$ for both compositions. These results are consistent with suggestions that the ferromagnetism observed in certain oxide semiconductors may be carrier mediated.

DOI: 10.1103/PhysRevB.79.165208 PACS number(s): 75.50.Pp, 72.25.Dc, 75.70.Ak

I. INTRODUCTION

The potential technological applications of magnetic semiconductors to the field of spintronics have motivated the study of many promising systems, including (Ga,Mn)As (Refs. 1 and 2) and transition metal doped semiconducting oxides (DMSO).[3,4] Some of these latter systems have been predicted to exhibit room-temperature ferromagnetism,[5] which has been observed experimentally in Co doped TiO_2,[6] Co doped ZnO,[7] and Cr doped In_2O_3.[8] The origin of ferromagnetism in these DMSO materials remains controversial, in part because of the possibility of a magnetic signal arising from undetected transition metal oxide impurity phases.[9] At the same time, ferromagnetism has been observed in a number of undoped oxide samples including HfO_2,[10] TiO_2,[11] and In_2O_3.[11] However, attempts to reproduce these results on undoped samples have not always been successful, leading to considerable uncertainty concerning magnetism in these materials.

In_2O_3 is a transparent semiconductor and can be highly conductive at room temperature when doped, making ferromagnetic In_2O_3 films attractive candidates for magneto-optical and spintronic devices. Room-temperature ferromagnetism has been predicted for Mo doped In_2O_3 films[12] and observed in Ni, Fe, and Co doped samples[13] as well as undoped In_2O_3.[11] It has been shown that the electrical and magnetic properties of $Cr:In_2O_3$ films are both sensitive to the oxygen vacancy defect concentration and that the ferromagnetic interaction depends on carrier density.[8] While it has been suggested that ferromagnetism in $Cr:In_2O_3$ films is carrier mediated,[14] the precise relationship between the spin transport properties of the charge carriers and the net ferromagnetic moment remains unclear. In this paper we demonstrate that the charge carriers in undoped In_2O_3 films have a significant spin polarization at helium temperatures.

II. MATERIALS AND METHODS

We prepared ceramic samples of In_2O_3 (with a base purity of 99.99%) and In_2O_3 doped with 2 at % Cr using a standard solid-state process.[15] The powder samples were pressed into 2 in. diameter sputtering targets, then annealed in air at 1100 °C for 6 h. In_2O_3 and $Cr:In_2O_3$ thin films were deposited by reactive magnetron sputtering of this target using an rf power source. High-purity argon was used as the sputtering gas and a small partial pressure of oxygen was maintained to obtain stoichiometric films. Oxygen at a partial pressure of 10^{-3} torr and argon at a partial pressure of 1.4×10^{-2} torr were used as reactive and sputtering gases, respectively. The films were deposited onto (0001) oriented single crystal sapphire substrates, which have a small intrinsic magnetic background and are conducive to optical characterization of the films. The as-prepared samples were insulating and non- or very weakly magnetic. All films became conducting and ferromagnetic when annealed in vacuum for 6–8 h to add oxygen vacancies. We found that vacuum annealing the samples for shorter times, from 2 to 5 h, still produced ferromagnetic samples, but yielding somewhat smaller ($\approx$25% relative decrease) magnetizations.

The x-ray diffraction (XRD) spectra for the In_2O_3 and $Cr:In_2O_3$ samples are shown in Fig. 1(a). The polycrystalline films are textured, with strong diffraction peaks indicating a preferred orientation along (222) or (400). There is no evidence for secondary phase formation. The high-resolution transmission electron microscopy (HRTEM) image of a $Cr:In_2O_3$ film shown in Fig. 1(b) indicates the absence of defects, secondary phases, or clusters in these high-quality samples, with the exception of the clear grain boundaries seen in Figs. 1(c) and 1(d). The well-defined lattice fringes at 2.92 Å are consistent with a (222) orientation for the sample. Figure 1(c) shows an image of a typical region in the grain boundaries in the $Cr:In_2O_3$ film. We do not observe any evidence for secondary phases developing in these regions. We show a cross-sectional TEM image in Fig. 1(d), which indicates that the film has a regular, columnar growth. The difference in the contrast at the grain boundaries and the grain interiors of the bright field image in Fig. 1(d) indicates that there can be preferential etching of the film during ion-beam milling HRTEM studies on undoped In_2O_3 samples showing qualitatively similar features. We focus on presenting the data on the $Cr:In_2O_3$ samples here since these samples would be most likely to express secondary impurity phases due to the presence of the Cr dopant ions.

Previous studies have established Raman spectroscopy as a powerful tool for identifying impurity phases in doped ox-

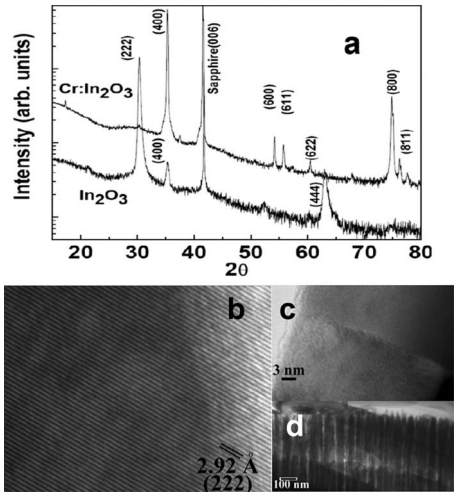

FIG. 1. (a) X-ray diffraction spectrum for a pure In_2O_3 sample (lower curve) and a Cr doped to 2 at % In_2O_3 thin film (upper curve). (b) HRTEM of the $Cr:In_2O_3$ thin film, showing the crystalline structure and absence of any impurity phase. (c) HRTEM image of a grain boundary in the film, which shows no evidence for any secondary phase precipitation. (d) Cross-sectional TEM image showing the highly textured thin film.

ide semiconducting materials.[16] In order to more carefully search for very small amounts of impurity phases, which could fall below the XRD detection limit or be missed in the local HRTEM studies, we also conducted extensive Raman studies on these films. We plot a representative Raman spectrum for $Cr:In_2O_3$ in Fig. 2, together with a spectrum measured for Cr_2O_3, the most stable oxide of Cr. In the In_2O_3 spectrum, we observe Raman bands at ≈ 305 cm^{-1}, 367 cm^{-1}, 496 cm^{-1}, and 628 cm^{-1}; these positions and intensities are characteristic of the standard Raman spectra expected for In_2O_3.[17] The Raman spectrum of the Cr_2O_3 sample shows a sharp peak centered at ≈ 549 cm^{-1} which

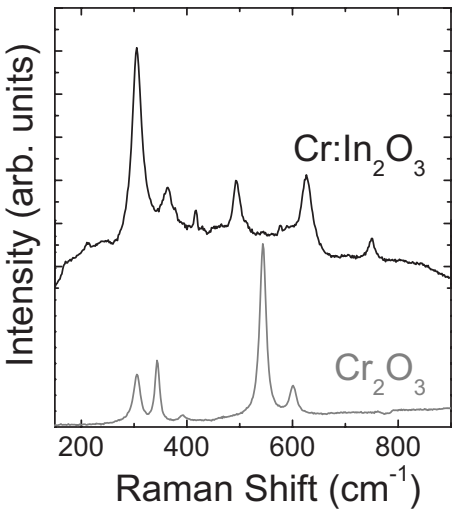

FIG. 2. Raman spectra for the $Cr:In_2O_3$ thin-film sample (upper curve, black) and bulk Cr_2O_3 (bottom curve, gray). The vertical scale for the two curves is different and the curves have been offset for clarity.

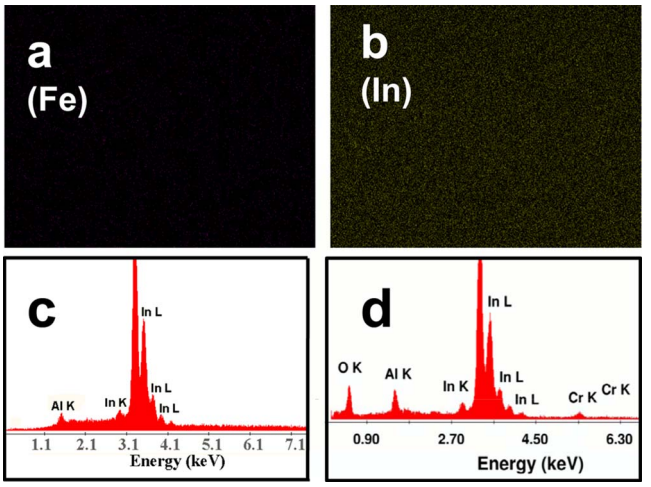

FIG. 3. (Color online) Representative SEM EDAX area scans of the In_2O_3 film for (a) Fe and (b) In. (c) EDAX spectrum for the In_2O_3 film. (d) EDAX spectrum for the $Cr:In_2O_3$ film showing the presence of Cr in this sample.

corresponds to the A_{1g} mode of Cr_2O_3.[18] Since the A_{1g} Raman peak of Cr_2O_3 is strong,[19] Raman spectroscopy provides higher sensitivity to identify any small amount of the Cr_2O_3 phase in In_2O_3 compared to x-ray diffraction technique. As a final check to rule out the possible presence of macroscopic impurity phases in the In_2O_3 and $Cr:In_2O_3$ films, we used scanning electron microscopy energy dispersive x-ray analysis (SEM EDAX) to do area measurements of the transition metal concentrations, including Cr, Co, Fe, Ni, and Mn. Figures 3(a) and 3(b) show representative scans for Fe and In in an In_2O_3 film. We find no evidence for any Fe signal above background. Similar scans for the other transition metals show no indication of any signal. We plot the spectrum for the In_2O_3 and $Cr:In_2O_3$ films in Figs. 3(c) and 3(d), respectively. In both, we see only peaks corresponding to In, O, Al, and Cr (for the $Cr:In_2O_3$ sample), with the Al signal coming from the sapphire substrate. Taken collectively, these studies rule out the possibility of any significant accidental contamination of the In_2O_3 and $Cr:In_2O_3$ films with magnetic transition metal impurities.

III. RESULTS AND DISCUSSION

We plot the temperature-dependent electrical resistivity for both the In_2O_3 and $Cr:In_2O_3$ samples in Fig. 4(a). These data were obtained on 1.1 μm thick samples after vacuum annealing. Room-temperature Hall measurements estimate the carrier concentration to be 6×10^{19} cm^{-3} for the In_2O_3 films and 3.5×10^{20} cm^{-3} for the $Cr:In_2O_3$ films. Both the In_2O_3 and $Cr:In_2O_3$ films remain conductive down to low temperatures and exhibit qualitatively identical behavior. Similar temperature dependence with a minimum in $\rho(T)$ has been observed in other doped oxide semiconductors, including Ga doped ZnO,[20] where the metallic conductivity at high temperatures is attributed to the highly degenerate nature of the samples.

We measured the in-plane magnetization of these thin-film samples using a high-sensitivity Quantum Design

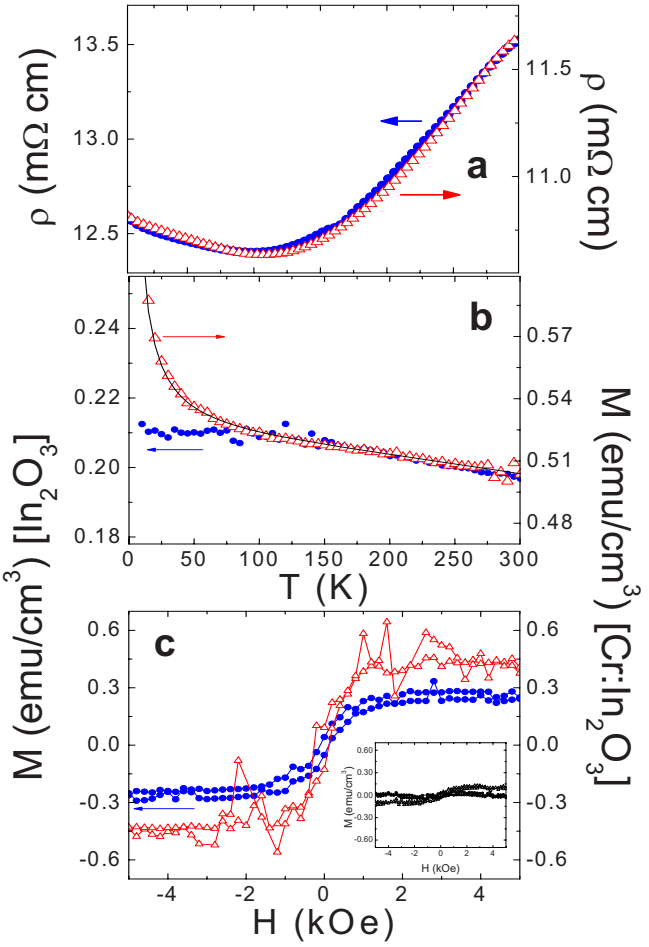

FIG. 4. (Color online) (a) Resistivity vs temperature for the vacuum annealed In_2O_3 and $Cr:In_2O_3$ samples. (b) Magnetization measured as a function of temperature for an In_2O_3 film and a $Cr:In_2O_3$ film, measured in a magnetic field of 1 kOe. The solid line is the fit to a Curie impurity tail, as described in the text. (c) Magnetization vs magnetic field measured at $T=300$ K for an In_2O_3 film and a $Cr:In_2O_3$ film. Inset: $M(H)$ for a representative as-prepared In_2O_3 film (black circles) and the as-prepared $Cr:In_2O_3$ film (black triangles) prior to vacuum annealing. The scale for the inset is the same as the scale for the main panel. For all panels, the vacuum annealed In_2O_3 data are shown with filled (blue) circles and the vacuum annealed $Cr:In_2O_3$ data are shown with open (red) triangles.

MPMS magnetometer. These magnetic data have been corrected for a small diamagnetic background from the sapphire substrate. The as-prepared films are non- or weakly magnetic, as shown in the inset to Fig. 4(c). The moment of a representative as-prepared undoped In_2O_3 sample is negligible, but the as-prepared $Cr:In_2O_3$ film shows a small magnetization. We attribute this weak ferromagnetism to the presence of some incidental oxygen vacancy defects introduced during synthesis. We plot the temperature-dependent magnetization for the vacuum annealed In_2O_3 and $Cr:In_2O_3$ films in Fig. 4(b). The magnetizations for both samples exhibit very similar behavior and are almost temperature independent at higher temperatures, with the $Cr:In_2O_3$ sample showing a noticeable increase only at temperatures below 25 K. We attribute this upturn to a Curie tail arising from paramagnetic Cr ions in the sample, which are absent in the In_2O_3 film. Fitting this upturn to a Curie susceptibility plus a spin-wave term as $M(T)=M_0+HC/T+M_S(1-BT^{3/2})$ with M_0 as a constant background, C as a Curie term, and B as the spin-wave stiffness, as shown in Fig. 4(b), we find that this anomaly can be accounted for by $\approx 75\%$ of the Cr ions remaining paramagnetic. The Curie temperature estimated for $Cr:In_2O_3$ from this fit is approximately $T_C=630$ K.

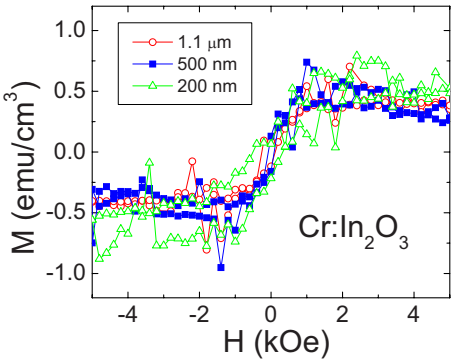

FIG. 5. (Color online) Magnetization curves for $Cr:In_2O_3$ films having thickness ranging from 200 to 1100 nm, measured at $T=300$ K.

We plot the room-temperature magnetization curves for a vacuum annealed In_2O_3 film and for both as-prepared and vacuum annealed $Cr:In_2O_3$ films in Fig. 4(c). Both vacuum annealed samples exhibit clear hysteresis loops consistent with room-temperature ferromagnetic order. The vacuum annealed In_2O_3 film shows a saturation magnetization of approximately 0.3 ± 0.1 emu/cm^3 while the vacuum annealed $Cr:In_2O_3$ sample has a magnetization of 0.5 ± 0.1 emu/cm^3. This magnetization is approximately one order of magnitude smaller than observed in other $Cr:In_2O_3$ films,[8] which we attribute to differences in the techniques used to prepare the samples.

We measured room-temperature magnetization curves for $Cr:In_2O_3$ films of different thickness. These results are plotted in Fig. 5. We found that the volume magnetization was approximately the same for all three films. This result suggests that the magnetism is not simply an interfacial effect but develops throughout the volume of the sample. More significantly, this consistency between the different measurements helps to confirm that the ferromagnetic signal is not produced by impurities accidentally deposited during sample preparation or annealing, since these would not be expected to show a systematic dependence on film thickness.

In order to investigate the coupling between the charge carriers and the ferromagnetic moment in the In_2O_3 and $Cr:In_2O_3$ films we used PCAR spectroscopy,[21,22] which has recently emerged as a viable technique to directly measure the transport spin polarization in magnetic materials[23] including dilute magnetic semiconductors.[24,25] The PCAR technique is based on the sensitivity of the quasiparticle-supercurrent conversion process (Andreev reflection) at a superconductor/normal contact to the degree of spin imbalance.

All of the measured Sn/In_2O_3 and $Sn/Cr:In_2O_3$ contacts exhibit characteristic conductance curves, with the dip at

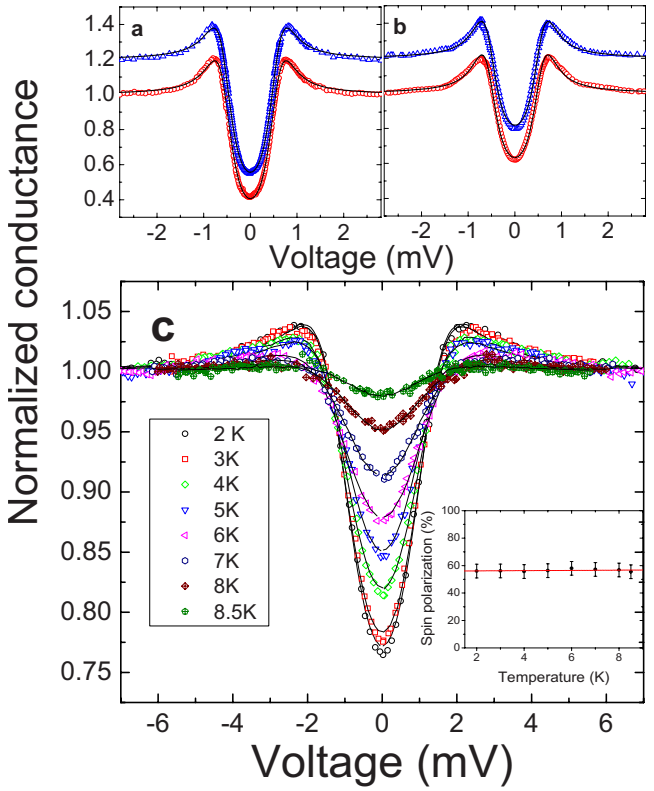

FIG. 6. (Color online) (a) and (b) Normalized conductance curves for two different Sn contacts for (a) $Cr:In_2O_3$ and (b) In_2O_3 samples at $T=1.2$ K. One curve in each plot is offset for clarity. Solid lines are the numerical fits obtained with the diffusive model using the BCS gap of bulk Sn, $\Delta=0.57$ meV. (a) Contact resistance $R_c=48\ \Omega$ (open circles) with fitting parameters: $Z=0.44$ and $P=47\%$; $R_c=35\ \Omega$ (open triangles) with $Z=0.47$ and $P=52\%$. (b) $R_c=75\ \Omega$ (open circles) with $Z=0$ and $P=40\%$; $R_c=87\ \Omega$ (open triangles) with $Z=0$ and $P=42\%$ (c) A single Nb contact with the In_2O_3 thin film at different temperatures ($R_c=61\ \Omega$). The BCS temperature dependence of the gap with $\Delta(0)=1.2$ mV was used for all the fits. The inset shows the temperature dependence of the resulting spin polarization in In_2O_3 with an average $P=56\%$.

zero bias voltage indicating the suppression of Andreev reflection due to spin polarization of the current. Figures 6(a) and 6(b) show representative conductance curves for two different contacts for both the In_2O_3 and $Cr:In_2O_3$ films measured in Fig. 4. The data are analyzed using the BCS gap of bulk Sn, which at the measurement temperature of $T=1.3$ K is approximately 0.57 meV. Additional contribution to the spreading resistance of the films—in the range of 20–40 Ω at 2 K—has been included in our analysis.[26]

Using a typical value for the contact resistance of 50 Ω, we estimate the contact size d (Ref. 27) to be much larger than the mean free path L. Accordingly, we have used the diffusive limit of Ref. 28 to analyze these data. The interface barrier strength Z is generally quite low, $Z\leq 0.4$ and there is no evidence for any polarization dependence on Z. This analysis, averaged over a number of different point contacts in several samples, yields a spin polarization of $45\%\pm 5\%$ and $\approx 50\%\pm 5\%$ in the In_2O_3 and $Cr:In_2O_3$ samples, respectively. We note that this robust spin polarization is compatible with the small observed magnetic moment, as the carrier

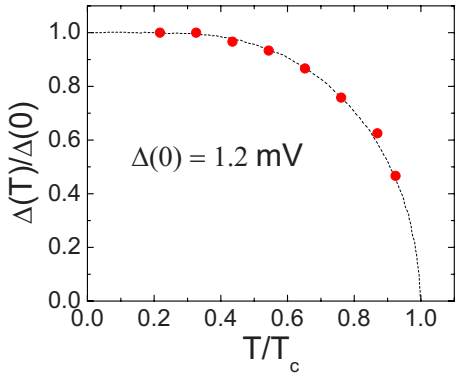

FIG. 7. (Color online) Temperature dependence of the Nb gap parameter used to fit the PCAR measurements (solid symbols). The dashed line shows the best fit to a BCS temperature dependence.

density in these films is also small, only on the order of $n=10^{20}/\mathrm{cm}^3$.

We have also performed a series of measurements in In_2O_3 at different temperatures using a Nb tip. These data, shown in Fig. 6(c), show that the magnitude of the zero bias dip decreases as the superconducting transition temperature for Nb is approached [Fig. 6(c)]. We plot the temperature dependence of the superconducting gap parameter determined from fitting of the PCAR data in Fig. 7. The temperature dependence is consistent with that expected for a BCS superconductor, but the zero-temperature gap is 1.2 meV, somewhat smaller than the 1.5 meV expected for Nb. We attribute this gap reduction to the inelastic scattering in the contact area,[24] which is also consistent with the small thermal broadening we observe. From these measurements, we obtained a spin polarization of ≈55% over the entire temperature range, as expected for temperatures well below the Curie temperature as shown in the inset to Fig. 6(c).

The observation of carrier-mediated ferromagnetism coexisting with n-type conductivity in In_2O_3 poses a serious theoretical challenge. While it has been established that oxygen vacancies are the most abundant intrinsic (donor) defects in In_2O_3 and can account for its room-temperature conductivity,[29] they alone are unlikely to produce ferromagnetism.[30] It has been proposed that cation vacancies could be responsible for the observed ferromagnetic properties of nonmagnetic oxides.[30–32] It is also known that In_2O_3 is highly compensated, with the concentration of the free carriers to the donor defects of about 1:5.[33] Based on the experimentally observed n-type conductivity of the films, we assume that In_2O_3 films are self-doped with donors (oxygen vacancies) of density N_d and self-compensated by magnetic acceptors (indium vacancies) of density $N_s \lesssim N_d$. Due to this inequality all of the acceptors are negatively charged and carry spin $J=1$. The interaction between the electron spins $\vec{s}_i$ and the localized acceptor spins $\vec{J}_j$ is

$$H_{\mathrm{ex}} = -\Gamma_{\mathrm{ex}} \sum_{i,j} \delta(\vec{r}_i - \vec{R}_j)\vec{s}_i \cdot \vec{J}_j, \qquad (1)$$

where Γ_{ex} is the exchange coupling and $\vec{r}_i$ ($\vec{R}_j$) is the position of the carrier (acceptor). The carriers can reside either in

delocalized conduction states or in localized states of the neutral donors. Ordering of the localized acceptor spins will split the conduction band leading to a nonzero spin polarization of the conduction electrons. Our main assumption is that the donors form a very narrow resonant impurity band above the bottom of the conduction band.[29] The existence of such states in ionic crystals has been predicted theoretically.[34] Due to a very strong electron-lattice interaction the resonant states can be treated as purely localized ones with almost infinite effective mass. While the neutral donors forming the impurity band carry the spin, the associated electrons will not contribute to the transport due to their extremely low mobility. The density of the donors residing in the impurity band and mediating magnetism is $N_d \sim (2-4)\times 10^{21}$ cm^{-3} with only a fraction $\sim(5-10)\times 10^{19}$ cm^{-3} of the donor electrons populating the conduction band. This explains the observed high Curie temperature at fairly modest carrier concentrations. It is well known that a very high density of states (DOS) at the Fermi level rather than the strength of the exchange interaction is primarily responsible for the high Curie temperatures of the transitional metals.[35] In our case this DOS is formed by the quasilocalized donor states. We emphasize that while it is the impurity band electrons that are mostly responsible for mediating magnetism, this is only possible when $N_d > N_s$, so the development of ferromagnetic order is intimately related to the presence of conduction electrons. Using the self-consistent equation for the spin density, M, of the In vacancies, we find[36]

$$M = N_s J B_J[\beta J \Gamma_{\rm ex}(S + \nu S_d)]. \tag{2}$$

Here N_s is the number of In vacancies per unit volume, S and S_d are the spin densities of the free and donor (impurity band) electrons given by

$$S = (1/2) N_c(\beta) G_-(\beta\mu, \beta\Delta), \tag{3}$$

with G_- as a function of the Fermi integral defined in the following, and

$$S_d = \frac{N_d \sinh(\beta\nu\Delta/2)}{\exp[\beta(\epsilon_d - \mu)] + 2\cosh(\beta\nu\Delta/2)}, \tag{4}$$

respectively, where $\Delta = \Gamma_{\rm ex} M$ is the Zeeman splitting of the conduction band, $\beta = (k_B T)^{-1}$, $N_c(\beta) = 2.5 \times 10^{19}$ cm$^{-3}(m^*/m_0)^{3/2}(300\ {\rm K}\beta)^{-3/2}$, N_d is the number of donors per unit volume, ϵ_d is the donor energy level (impurity band), and μ is the chemical potential. All energies are counted from the bottom of the conduction band.

The parameter ν reflects the short-range character of the exchange interaction between acceptor and donor spins, which results in the reduction of the donor Zeeman splitting. Technically ν has to be either estimated from percolation theory[36] or calculated by Monte Carlo methods. In our calculations we used it as a fitting parameter and found $\nu = 0.7$. For notational simplicity, we define $G_\pm$, a function of the Fermi integral, as

$$G_\pm(x,y) = \frac{1}{2}[F_{1/2}(x + y/2) \pm F_{1/2}(x - y/2)] \tag{5}$$

with $F_j(\eta)$ as the Fermi integral of order $j (j = 1/2)$,

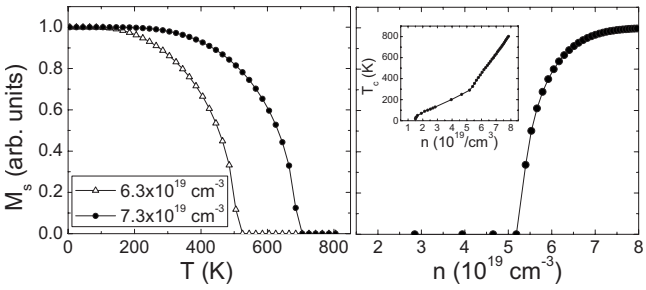

FIG. 8. (Left panel) Magnetization vs temperature for different carrier concentrations. The open triangles are calculated for a carrier concentration of 6.3×10^{19} cm^{-3} while the closed circles are for 7.3×10^{19} cm^{-3}. (Right panel) Room-temperature magnetization vs carrier concentration. Inset: ferromagnetic Curie temperature plotted as a function of carrier concentration.

$$F_j(\eta) = \frac{1}{\Gamma(j+1)} \int_0^\infty \frac{\xi^j d\xi}{1 + \exp(\xi - \eta)}, \tag{6}$$

and x and y as placeholder arguments for the function $G_\pm$.

The chemical potential μ can be found from the electroneutrality condition, $N_d^+ = n + N_s$, or explicitly

$$\frac{\exp[\beta(\epsilon_d - \mu)]}{\exp[\beta(\epsilon_d - \mu)] + 2\cosh(\beta\nu\Delta/2)} = N_c(\beta) G_+(\beta\mu, \beta\Delta) + N_s. \tag{7}$$

This expression can be used to estimate the magnetization in In_2O_3 for a range of parameters. In Fig. 8(a) we plot the predicted temperature dependence of the magnetization for two carrier concentrations, and in Fig. 8(b) we plot the dependence of the magnetization on carrier concentration at room temperature. Both calculations use the parameters $\epsilon_d = 140$ meV, $m^*/m_0 = 0.5$, $\Gamma_{\rm ex} = 70$ meV nm^3, and $N_s = 2 \times 10^{21}$ cm^{-3}. We find that the magnetization is relatively temperature independent at low temperatures with a magnitude depending only weakly on carrier concentration for concentrations well above the critical threshold, consistent with the experimental observations. We plot the predicted Curie temperature as a function of carrier concentration in the inset to Fig. 8(b). This model predicts that room temperature ferromagnetism in undoped In_2O_3 should develop above a critical carrier concentration of approximately 4×10^{19} cm^{-3}, consistent with our observation that the as-prepared samples are nonferromagnetic, but as the carrier concentration is increased to $\approx 10^{20}$ cm^{-3} a robust ferromagnetic moment develops. Intriguingly, this model would also predict that ferromagnetism should develop only below room temperature for a relatively narrow concentration of carrier concentrations between roughly 2×10^{19}/cm^3 and 3×10^{19}/cm^3. We have not observed the onset of ferromagnetic order below room temperature in any of our In_2O_3 or $Cr:In_2O_3$ films, which we attribute to the restricted range of carrier concentrations exhibiting this behavior.

In conclusion, we have established that vacuum annealed In_2O_3 thin films exhibit ferromagnetic order and that the charge carriers exhibit a sizeable spin polarization at $T = 1.3$ K. Our direct measurement of the spin polarization

using PCAR spectroscopy shows a spectrum characteristic of the interface between a superconductor and ferromagnet, with a spin polarization of $\approx 50\%$ for both In_2O_3 and $Cr:In_2O_3$ samples. The close agreement between both the magnetic and transport measurements for In_2O_3 and $Cr:In_2O_3$ strongly suggests that the presence of magnetic transition metal dopant ions is not necessary to produce carrier-mediated ferromagnetism in this system. The observation of a finite spin polarization points to a strong coupling between the charge carriers and the ferromagnetic moment. While our conceptual model is by no means complete, and would require additional experimental and computational work to verify, it predicts the carrier concentration threshold above which room-temperature ferromagnetism emerges, consistent with our experimental observations. This study confirms one of the principal assumptions underlying the study of room-temperature ferromagnetism in dilute magnetic semiconducting oxides, namely, that the charge carriers themselves are spin polarized.

ACKNOWLEDGMENTS

This work was supported by the National Science Foundation under NSF CAREER Grants No. DMR-06044823 and ECS-0239058, by DARPA through ONR Grant No. N00014-02-1-0886, by ONR Grant No. N00014-06-1-0616, by NSF Grant No. ECCS-0725881, by the Institute for Materials Research at Wayne State University, and by the Jane and Frank Warchol Foundation.

*Permanent address: LPCES, CNRS, ICMMO, Universite Paris-Sud, 91405 Orsay, France.

[1] S. A. Wolf, D. D. Awschalom, R. A. Buhrman, J. M. Daughton, S. von Molnar, M. L. Roukes, A. Y. Chtchelkanova, and D. M. Treger, Science **294**, 1488 (2001); I. Zutic, J. Fabian, and S. Das Sarma, Rev. Mod. Phys. **76**, 323 (2004).
[2] A. H. MacDonald, P. Schiffer, and N. Samarth, Nature Mater. **4**, 195 (2005).
[3] J. M. D. Coey, Curr. Opin. Solid State Mater. Sci. **10**, 83 (2006).
[4] S. A. Chambers, Surf. Sci. Rep. **61**, 345 (2006).
[5] T. Dietl, H. Ohno, F. Matsukura, J. Cibert, and D. Ferrand, Science **287**, 1019 (2000).
[6] Y. Matsumoto, M. Murakami, T. Shono, T. Hasegawa, T. Fukumura, M. Kawasaki, P. Ahmet, T. Chikyow, S. Koshihara, and H. Koinuma, Science **291**, 854 (2001).
[7] S. B. Ogale, R. J. Choudhary, J. P. Buban, S. E. Lofland, S. R. Shinde, S. N. Kale, V. N. Kulkarni, J. Higgins, C. Lanci, J. R. Simpson, N. D. Browning, S. Das Sarma, H. D. Drew, R. L. Greene, and T. Venkatesan, Phys. Rev. Lett. **91**, 077205 (2003).
[8] J. Philip, A. Punnoose, B. I. Kim, K. M. Reddy, S. Layne, J. O. Holmes, B. Satpati, P. R. Leclair, T. S. Santos, and J. S. Moodera, Nature Mater. **5**, 298 (2006).
[9] D. W. Abraham, M. M. Frank, and S. Guha, Appl. Phys. Lett. **87**, 252502 (2005).
[10] M. Ventkatesan, C. B. Fitzgerald, and J. M. D. Coey, Nature (London) **430**, 630 (2004).
[11] N. H. Hong, J. Sakai, N. Poirot, and V. Brize, Phys. Rev. B **73**, 132404 (2006).
[12] J. E. Medvedeva, Phys. Rev. Lett. **97**, 086401 (2006).
[13] G. Peleckis, X. Wang, and S. X. Dou, Appl. Phys. Lett. **89**, 022501 (2006).
[14] H. Raebiger, S. Lany, and A. Zunger, Phys. Rev. Lett. **101**, 027203 (2008).
[15] P. Kharel, C. Sudakar, M. B. Sahana, G. Lawes, R. Suryanarayanan, and R. Naik, J. Appl. Phys. **101**, 09H117 (2007).
[16] C. Sudakar, J. S. Thakur, G. Lawes, R. Naik, and V. M. Naik, Phys. Rev. B **75**, 054423 (2007).
[17] W. B. White and V. G. Keramidas, Spectrochim. Acta A Mol. Biomol. Spectrosc. **28**, 501 (1972).
[18] S. H. Shim, T. S. Duffy, R. Jeanloz, C. S. Yoo, and V. Iota, Phys. Rev. B **69**, 144107 (2004).
[19] J. Mougin, N. Rosman, G. Lucazeau, and A. Galerie, J. Raman Spectrosc. **32**, 739 (2001).
[20] V. Bhosle, A. Tiwari, and J. Narayan, J. Appl. Phys. **100**, 033713 (2006).
[21] R. J. Soulen Jr., J. M. Byers, M. S. Osofsky, B. Nadgorny, T. Ambrose, S. F. Cheng, P. R. Broussard, C. T. Tanaka, J. Nowak, J. S. Moodera, A. Barry, and J. M. D. Coey, Science **282**, 85 (1998).
[22] S. K. Upadhyay, A. Palanisami, R. N. Louie, and R. A. Buhrman, Phys. Rev. Lett. **81**, 3247 (1998).
[23] P. Chalsani, S. K. Upadhyay, O. Ozatay, and R. A. Buhrman, Phys. Rev. B **75**, 094417 (2007).
[24] R. P. Panguluri, K. C. Ku, T. Wojtowicz, X. Liu, J. K. Furdyna, Y. B. Lyanda-Geller, N. Samarth, and B. Nadgorny, Phys. Rev. B **72**, 054510 (2005).
[25] J. G. Braden, J. S. Parker, P. Xiong, S. H. Chun, and N. Samarth, Phys. Rev. Lett. **91**, 056602 (2003).
[26] G. T. Woods, R. J. Soulen, I. I. Mazin, B. Nadgorny, M. S. Osofsky, J. Sanders, H. Srikanth, W. F. Egelhoff, and R. Datla, Phys. Rev. B **70**, 054416 (2004).
[27] R. P. Panguluri, G. Tsoi, B. Nadgorny, S. H. Chun, N. Samarth, and I. I. Mazin, Phys. Rev. B **68**, 201307(R) (2003).
[28] I. I. Mazin, A. A. Golubov, and B. Nadgorny, J. Appl. Phys. **89**, 7576 (2001).
[29] Stephan Lany and Alex Zunger, Phys. Rev. Lett. **98**, 045501 (2007).
[30] J. Osorio-Guillen, S. Lany, S. V. Barabash, and A. Zunger, Phys. Rev. B **75**, 184421 (2007).
[31] I. S. Elfimov, S. Yunoki, and G. A. Sawatzky, Phys. Rev. Lett. **89**, 216403 (2002).
[32] C. Das Pemmaraju and S. Sanvito, Phys. Rev. Lett. **94**, 217205 (2005).
[33] J. L. Bellingham, A. P. Mackenzie, and W. A. Phillips, Appl. Phys. Lett. **58**, 2506 (1991).
[34] S. Lany and A. Zunger, Phys. Rev. B **72**, 035215 (2005).
[35] J. F. Janak, Phys. Rev. B **16**, 255 (1977).
[36] A. G. Petukhov, I. Zutic, and S. C. Erwin, Phys. Rev. Lett. **99**, 257202 (2007).